Die Grenzen der Chemie neu ausloten? It takes #HumanChemistry

Wir suchen kreative Chemikerinnen und Chemiker, die mit uns gemeinsam neue Wege gehen wollen – mit Fachwissen, Unternehmertum und Kreativität für innovative Lösungen. Informieren Sie sich unter:

evonik.de/karriere

evonik
Leading Beyond Chemistry

Current-Driven Organic Electrochemical Transistors for Monitoring Cell Layer Integrity with Enhanced Sensitivity

Katharina Lieberth, Paolo Romele, Fabrizio Torricelli, Dimitrios A. Koutsouras, Maximilian Brückner, Volker Mailänder, Paschalis Gkoupidenis, and Paul W. M. Blom*

In this progress report an overview is given on the use of the organic electrochemical transistor (OECT) as a biosensor for impedance sensing of cell layers. The transient OECT current can be used to detect changes in the impedance of the cell layer, as shown by Jimison et al. To circumvent the application of a high gate bias and preventing electrolysis of the electrolyte, in case of small impedance variations, an alternative measuring technique based on an OECT in a current-driven configuration is developed. The ion-sensitivity is larger than 1200 mV V^{-1}dec^{-1} at low operating voltage. It can be even further enhanced using an OECT based complementary amplifier, which consists of a p-type and an n-type OECT connected in series, as known from digital electronics. The monitoring of cell layer integrity and irreversible disruption of barrier function with the current-driven OECT is demonstrated for an epithelial Caco-2 cell layer, showing the enhanced ion-sensitivity as compared to the standard OECT configuration. As a state-of-the-art application of the current-driven OECT, the in situ monitoring of reversible tight junction modulation under the effect of drug additives, like poly-L-lysine, is discussed. This shows its potential for in vitro and even in vivo toxicological and drug delivery studies.

1. Organic Bioelectronics: A Field with an Impressive Perspective

Utilizing electronic circuits to detect or stimulate biological systems is understood as the field of bioelectronics. The famous experiment of Luigi Galvani in the 1780s was the first step into bioelectronic research, investigating the movement of a sciatic nerve of detached frogs´ legs upon applied potential of an inorganic electrode. As the field of organic bioelectronics grew exponentially over the last 30 years, more and more applications for biology were developed and complement the inorganic counterpart. The translation of biochemical signals is crucial, as it portrays numerous regulating and defense mechanisms in humans and animals represented by small cations[1] (nutrients) and neurotransmitters (hormones),[2] but also macromolecules (DNA[3] and proteins[4]). State-of-the-art optical techniques, like immunofluorescence staining and permeability assays, have drawbacks, like the spatio-temporal resolution together with biocompatibility, invasiveness, and time-consuming processability.[5,6] To answer to-days questions non-invasive devices are of great need, allowing in vitro and in vivo studies in the medical domains of therapy, diagnostics, cell biology, and health care monitoring, for example, pacemaker, deep brain stimulator, or cochlear implants. Organic bioelectronic devices are a promising candidate to overcome these challenges, as they have the ability to bridge the signaling gap between biology and technology due to their high biocompatibility and the possibility to tailor physical properties of the organic electronic conducting material (OEM) due to organic synthesis. Besides humans, organic bioelectronics also found relevant applications considering fungi, plants,[7] bacteria,[8] protista, and archaea systems.[9] Organic bioelectronic devices contain an OEM in various device architectures, such as permeable/semipermeable membranes on electrodes, semiconductors, and conductors in transistors and as insulators.[9] Being biocompatible and having the ability to tailor physical properties like ion-sensitivity, stretchability, or stability in aqueous electrolyte according to the sensing application by organic synthesis, makes them the workhorse of organic bioelectronics.

K. Lieberth, D. A. Koutsouras, M. Brückner, V. Mailänder, P. Gkoupidenis, P. W. M. Blom
Max Planck Institute for Polymer Research
Ackermannweg 10, Mainz 55128, Germany
E-mail: blom@mpip-mainz.mpg.de
P. Romele, F. Torricelli
Department of Information Engineering
University of Brescia
Via Branze 38, Brescia 25123, Italy
M. Brückner, V. Mailänder
Dermatology Clinic
University Medical Center of the Johannes Gutenberg-University Mainz
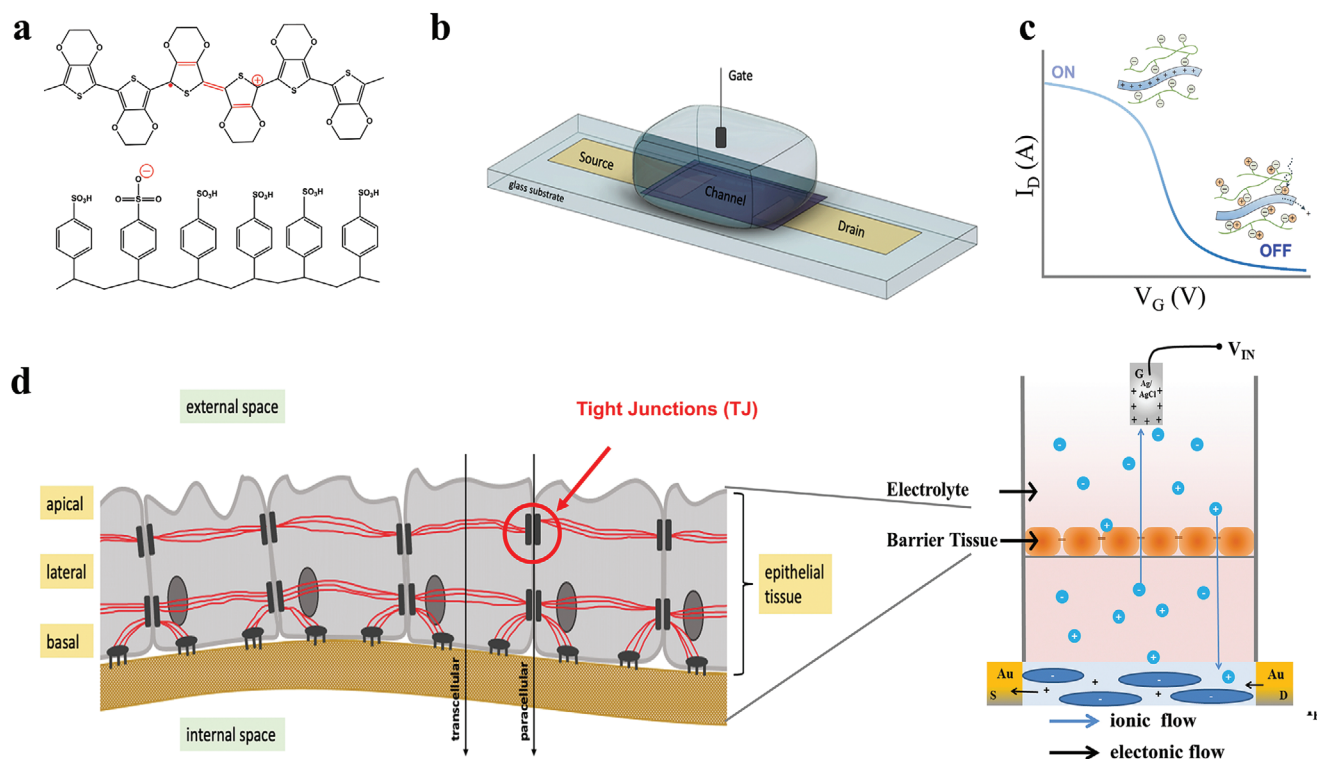Langenbeckstr. 1, Mainz 55131, Germany

Figure 1. The OECT and its application as an impedance sensor. a) Molecular structure of positively doped conducting polymer PEDOT (up) and the negatively charged polyelectrolyte PSS (down). b) Device architecture of the OECT. c) Working principle of a p-type OECT with PEDOT:PSS as CP, operating in depletion mode. Reproduced with permission.[31] Copyright 2018, Springer Nature. d) Impedance sensing of barrier tissue (left) on a permeable filter, implemented in the OECT in a self-standing architecture (right). Reproduced with permission.[108] Copyright 2021, Wiley-VCH GmbH.

1.1. Mixed Ion-Electron Conductors: The Workhorse in Organic Bioelectronics

Small molecules and more important conducting polymers (CPs) are utilized as electron conductive material in organic bioelectronics, transporting either electrons (n-type) or holes (p-type). The first explored biocompatible CPs were the hole conducting polymers polypyrrole (PPy)[10] and poly(3,4-ethylenedioxythiophene) (PEDOT).[11,12] Both CPs can be obtained from monomer solutions together with their counterions by electro-polymerization or by polymeric chain reaction.[11–14] Positively doped CPs, by removing one electron, have a high electric conductivity across the volume, due to large charge delocalization over the CP´s π-orbitals. The semiconducting polymer PEDOT gained increasing attention over PPy due to its enhanced water stability, although it is only water soluble together with its counterion.[15] The dopant counterion stabilizes the doping state of PEDOT in aqueous electrolyte, being hydrophilic, but also promotes ion permeability throughout the whole volume of PEDOT:PSS films due to the porous morphology.[15–17] As counterion for PEDOT the anionic polyelectrolyte poly(styrene sulfoxide) (PSS) (**Figure 1a**) was established, providing high stability and ion permittivity.[18] PSS forms an amorphous backbone, in which PEDOT-rich domains are embedded. By applying positive gate bias, cations from the electrolyte are driven into the whole volume of the CP and thus dedope PEDOT. PEDOT:PSS therefore transduces ion flux into electronic cur-

rent, as PEDOT is electrochemically reduced by the penetration of cations into the PEDOT:PSS film, and oxidized again when cations are removed from the film. Since PEDOT:PSS can transport both ionic and electronic charges, it is called mixed ion-electron conductor.[19,20] The ionic conductance of the polymer is determined by the density and morphology of the PSS phase while the electronic conductance is determined by the structural and physical properties of the PEDOT phase.[15,16,21] As ions penetrate into the whole volume of the CP film, the electronic conductivity is a volumetric property. P-type doped CP-films operate in depletion mode. Vice versa n-type CPs, such as pristine poly-benzimidazobenzophenanthrolin, operate in accumulation mode.

Relevant features for bioelectronic operation are the operation at voltages well-below 1 V and stability in liquid environment. PEDOT:PSS provides these properties, accompanied by a flexible morphology, optical transparency, processability, and scalable green synthesis. In direct interface to tissues or cell layers, the soft and stretchable morphology of CPs enables achieving the ideal interface conditions, as is the case for PEDOT:PSS and PPy. Therefore, PEDOT:PSS finds wide application in electrophysiology and biosensing,[22,23] organic electrochemical transistors (OECTs) and electrodes for neuronal systems[14,23,24] as well as for organic electronic ion pumps.[25,26]

When PEDOT:PSS films interface aqueous electrolyte, water molecules form hydroxide bridges between the PSS backbones, which leads to film swelling. To prevent the decay in electric

**ADVANCED
SCIENCE NEWS**

www.advancedsciencenews.com

**ADVANCED
HEALTHCARE
MATERIALS**

www.advhealthmat.de

conductivity, polar organic solvents, such as dimethyl sulfoxide (DMSO) or ethylene glycol (EG), are added to concentrate the conducting PEDOT islands for conductivity improvement.[27] In case of DMSO the conductivity is two orders of magnitude larger as compared to PEDOT:PSS films in absence of DMSO.[28] Furthermore, silane-based crosslinkers, such as (3-glycidyloxypropyl) trimethoxysilane (GOPS), are added to enhance strechability and prevent dissolution and delamination of PEDOT:PSS films in aqueous solutions. Crosslinkers connect PSS backbones with each other and the glass surface.[29,30] Surfactants, such as Zonyl, improve the adhesion on substrates.

Over the last forty years various semi CPs of p- and n-type have been published.[31,32] However, the well-established PEDOT:PSS is in great focus with more than 15 000 publications per year,[33] being one of the most studied materials on earth, and it is the material of choice in the presented report. Due to the blue color in doped state and transparent color in undoped state, PEDOT has also been used as a pixel electrode in electrochromic displays.[34] Moreover, thanks to its high volumetric capacitance of the order of 40 F cm^{-3}, PEDOT:PSS finds application in ion-based energy storage systems like supercapacitors,[35] conducting channel of electrochemical transistors,[36] and sensors.[37] Today, PEDOT:PSS is also widely utilized as hole injecting electrode in organic light emitting diodes,[38] organic field effect transistors (OFET),[39] and hole extraction electrode in photovoltaics.[40]

1.2. The Base of Bioelectronics: PEDOT:PSS Coated Electrodes

Electrodes are the simplest device architecture and have extensively been studied for bioelectronic applications. Faradaic electrodes, like Ag/AgCl, reacting electrochemically with the electrolyte, are less applicable for biological applications, as the composition of the electrolyte changes and possibly released toxic compounds might harm biological tissue.[41] On the contrary, the usage of non-faradaic electrodes, like Au, forming an electric double layer (EDL) is preferred for bioelectronic applications. To effectively transduce ionic signals into electronic current, a low impedance at the electrode surface with a high ionic conduction is required. A porous CP film coated on the non-faradaic electrode surface is an attractive solution, having high electronic conductivity and ionic conductance. Moreover, the porous structure lowers the impedance of the electrode. The possibility of electropolymerization directly on the electrode eliminates photolithographic steps from the process and makes the film thickness finely controllable.[42] CP coated electrodes, especially PEDOT:PSS, found bioelectronic applications in neural activity sensing.[11,12] CP coatings enhance the electrical performance as well as biocompatibility of the electrode-tissue interface.[24] First in vivo experiments to heal diseases affecting the brain have been performed.[43]

1.3. Ion-Gated Organic Transistors

Coming from two-terminal to three-terminal device configurations, ion-gated organic transistors are essential devices in bioelectronics. Compared to conventional OFETs,[44] in ion-gated organic transistors the insulator is replaced with an electrolyte

and the conductivity of the organic semi-conducting channel is modulated by ions. Depending on the applied gate voltage (V_G), cations ($V_G < 0$ V) or anions ($V_G > 0$ V) are accumulated at the gate-electrolyte interface and a corresponding amount of anions or cations are accumulated at the electrolyte–semiconductor interface. More in detail, the ionic charges accumulated at the gate-electrolyte interface screen the charges in the metal gate, while the ionic charges accumulated at the electrolyte–semiconductor interface are electrostatically compensated by the electronic charge carriers (holes or electrons) induced into the semiconductor. In steady-state equilibrium conditions (i.e., no migration of ionic charges) the interface ionic-electronic charge compensation results in two EDLs at the corresponding interfaces (namely, gate-electrolyte and electrolyte–semiconductor), which are electrically equivalent to nanometer-thick capacitors. For EDL forming transistors typical values of the capacitance per unit area are in the range $1 \div 10 \times 10^{-6}$ F cm^{-2}, which is more than one order of magnitude larger than that obtained with conventional dielectrics. The large specific capacitance is due to the large permittivity of fluids and small radius of solvated ions (typically <1 nm). Depending on the electrolyte and organic semiconductor materials, the organic material can be impermeable or permeable to ions. In the case ions cannot penetrate the organic material a single electrolyte–semiconductor interface is formed giving rise to the class of electrolyte-gated organic field-effect transistors (EGOFETs).[45] EGOFETs are used to sense humidity,[46] pH,[47] DNA,[48] penicillin,[49] dopamine,[50] ions,[51] and the reaction of transmembrane proteins of a phospholipid layer.[52] In the case ions can penetrate the organic semiconductor, the EDL is distributed within the volume of the organic material giving rise to the class of OECTs.

2. The Raising Potential of the Organic Electrochemical Transistor

The first OECTs were developed by the Wrighton group in the 1980s, using polyaniline and poly(3-methylthiophene) as CPs.[53] In 2002 PEDOT:PSS was introduced by the Berggren group for OECTs and it is till now widely used as channel material for OECTs, especially in bioelectronics (Figure 1b).[19,31,54,55] The OECT with PEDOT:PSS as CP operates in depletion mode (Figure 1c). An important advantage of OECT is the volumetric capacitance due to the distributed EDL in the CPs, which results in a large transconductance (g_m), typically in the range of millisiemens, and, in turn, in an enhanced transduction and amplification of ionic signals into electronic currents. We note that the g_m of OECTs is about three orders of magnitude larger than that of OFETs.[22,23] However, the large overall capacitance results in a bandwidth limited to few kHz, which fortunately is not a major concern in bioelectronic applications. In the following section the already existing and promising future of OECTs in bioelectronics is drawn.

2.1. Device Structure: Materials and Fabrication Process

The OECT is a three terminal device consisting of a source and drain electrode, connected by the channel CP. The source-drain

ADVANCED
SCIENCE NEWS

www.advancedsciencenews.com

**ADVANCED
HEALTHCARE
MATERIALS**

www.advhealthmat.de

current I_D is modulated by ions penetrating from the electrolyte into the channel, driven by the gate potential. Typically, source and drain gold electrodes with a thin chromium adhesion layer below are deposited on a rigid substrate, like glass, using physical vapor deposition. Besides rigid on-chip technology, OECTs can be fabricated onto flexible substrates, such as PET, due to the mechanical properties of organic electronic materials as channel.[56] The work of Yao et al. shows that OECTs on flexible substrates have the advantage to monitor 3D microenvironments and obtain a similar signal-to-noise ratio to the one of OECTs on rigid substrate.[56] The merits of flexible OECTs for in vivo sensing are crucial, as first studies on sensing brain activity proved in 2012.[22] Flexible OECTs could monitor tissues[57] and reduce fabrication costs for in vitro chips by printing technologies.[58] Besides aqueous electrolyte, typically defined by a PMMA-well, the possibility to use solid electrolytes, using ionic liquids, offer a great potential for applications, for example, for wearable electronics, due to its wide variety of processing methods.[59] The channel geometries are determining the channel´s volumetric capacitance. Recently the group of Hsing et al. tuned the sensitivity of the OECT as an impedance sensor by optimizing the impedance relation of the channel and the integrated cell layer. It was found that an increased channel geometry enhances the sensitivity in the low frequency regime and therefore the suitability to monitor tightly packed cell layers. However, sensing leaky cell layers requires sensitivity in the high frequency regime, which is achieved with a small channel geometry.[60] The gate electrode is either deposited in plane on the substrate or as a top-electrode, for example, Ag/AgCl pellet, immersed into the electrolyte.[61] The voltage drop at the gate/electrolyte interface should be low, to have an efficient voltage transfer and thus, an efficient ion-to-electron transduction. A voltage loss means a reduction of the sensitivity of the OECT.[62] Ag/AgCl as a non-polarizable gate electrode achieves this due to electrochemical reaction of AgCl salt with plain silver or the electrolyte ions.[63] As a result, Ag/AgCl electrodes are widely used for biosensing short-time measurements.[56,64] Being easy to handle, but having the drawback of cytotoxic effects of Ag/AgCl on cells in the case of long-term measurements, the applications for top-gated OECTs for cell integrity are limited due to the formation of toxic Ag nanoparticles.[65,66] This drawback can be overcome by using a salt bridge, like saturated KCl solution, shielding the diffusion of AgCl into the electrolyte.[55,57,67] However, top-gated OECTs are not feasible to be used for in vivo applications. On-chip technology can be realized for OECTs using lateral electrodes, which enables not only in vitro but also in vivo cell integrity. As explained before polarizable materials, such as gold, are not suitable by themselves, but when coated with the electron-ion conducting polymer PEDOT:PSS,[67,68] a biocompatible operation and further advantages, such as a facile fabrication process, tunability of the device performance regarding gate and channel geometries, transparency to simultaneously record optical images, and flexibility to monitor 3D samples, are provided.[63,69–72]

2.2. Application of the OECT in Biology

Being biocompatible and stable in liquid environment, OECTs are in focus with the rise of bioelectronics.[9] Three main bioelec-

tronic applications of OECTs are i) electrophysiology and neural signal recordings,[73] ii) analyte detection with a functionalized gate electrode,[31] and iii) impedance sensing.[74] Indeed, OECTs can be placed in contact with human skin[75] for recording electrocardiograms or can be implanted in contact with organs in order to locally-amplify electrophysiological signals from the brain, heart, and muscles,[76] Works of the OECT in combination with different receptors or selective membranes showed the ability to detect, for example, ascorbic acid,[77] marine diatoms in the seawater medium,[78] dopamine,[79] acetylcholine, glutamate,[29] and proteins.[80] In the last decade, monitoring the integrity of barrier tissue got great attention.[5] Recently, OECTs found important application for monitoring the barrier tissues, sensing the resistance and capacitance of a cell layer being inserted between the gate and the channel.[55,64] In this progress report, we focus on OECTs for monitoring cell layer integrity with enhanced sensitivity.

3. The OECT as an Impedance Sensor

3.1. The Role of Tight Junctions in Barrier Tissues

Detecting disruption or malfunction of tissues is important for toxicological studies.[61,81] The studying of the reversible loss of barrier function offers great insights for the research on drug delivery and physiology in general. Confluent cell layers and tissues serving as physical barriers are so-called barrier tissues (Figure 1d). Epithelial barrier tissues cover the internal and external surfaces of organs, for example, the epidermal covering of skin, kidney, and gastrointestinal tract.[82] Protein complexes connect the cells of barrier tissue tightly, so that a semipermeable, physical barrier is formed separating the inner to the outer of the organ.[83] Hence, epithelial barrier tissues regulate the passage of nutrients from organs into blood, but restrict harmful substances.[84,85] The passage takes place either through cells (transcellular) or between adjacent cells (paracellular).[84] Epithelial cell layers are categorized in the apical, exposed to the external domain, the lateral, and the basal domain, connected to the matrix of the tissue. In the lateral part, cell–cell junctions are formed by various protein complexes, link the cytoskeleton of adjacent cells and determine the strength of barrier function of cell layers. The apical part facilitates absorption of nutrients. A closer look on the cell–cell junctions reveals four junctional complex types. Whereas for adherent junctions desmosomes are responsible for the cell layer stability, gap junctions enable the interchange of molecules between cells. However, tight junction (TJ) complexes regulate the exchange of ions and molecules paracellular through the barrier tissue by sealing the cell layer. Therefore, TJs define the paracellular barrier function.[83] In addition, TJs maintain cell polarity, by preventing apical and basal proteins to migrate to the other side.[83,86] They are dynamically modulated by the intracellular signaling transduction system of cells and a number of extracellular stimuli.[87,88] Tightness in epithelia alters according to the respective purpose of each tissue. The tightest barrier tissue is the blood–brain-barrier and the skin epithelium. A well-established model for the gastrointestinal tract, important for oral drug delivery is the epithelial colon carcinoma (Caco-2) cell line, found in the small intestine.[89] Transmembrane TJ complexes, like various claudin,

**ADVANCED
SCIENCE NEWS**

www.advancedsciencenews.com

**ADVANCED
HEALTHCARE
MATERIALS**

www.advhealthmat.de

occludin, tricellulin, and JAM proteins, mediate cell–cell adhesion, whereas cytoplasmic proteins, such as zonulin proteins, anchor transmembrane junctions to the actin cytoskeleton and are involved in recruiting regulatory proteins.[90–92]

The trans-epithelial resistance (TER) quantifies the barrier functionality of cell layers and tissues as figure-of-merit.[61,90,93] As an example the TER-value of barrier tissue from Caco-2 cell line is in the order of $\approx 500 \ \Omega \ cm^2$. Performing transepithelial electrical resistance measurements with a volt–ohm meter is one possibility to assess TER-values of cell layers. The paracellular conductance is measured using a two-electrode set-up. The basal and apical compartments connecting electrode and electrolyte are separated by a permeable Transwell-filter, on which cells are cultured.[72,94] Although this method is easy to handle, it suffers from low reproducibility and low temporal resolution.[61] The more advanced two-terminal frequency-dependent electrochemical impedance spectroscopy (EIS) determines the TER with higher reproducibility and higher sensitivity.[95] Less time-consuming automated EIS set-ups, such as the CellZScope, were evolved, measuring several samples in parallel.[96] Optical techniques like immunofluorescence spectroscopy or permeability assays are state-of-the-art techniques to visualize TJ proteins, utilizing antibody staining.[85,87,93,97] However, due to their invasiveness along with a low temporal resolution, in vivo applications are prohibited. Bioelectronics and specifically the OECT offer in vitro and in vivo impedance sensing with high sensitivity (HS) and temporal resolution (Figure 1d).

To improve drug targeting the detection and in situ monitoring of TJ modulation becomes crucial. Many clinically approved drugs are too big to paracellularly pass across barrier tissue and are repelled from TJs due to their hydrophobic nature, thus prohibiting the patient friendly oral intake of drugs.[90,91] Together with the development of hydrophilic drug delivery systems, agents to regulate the tightness of barrier tissue by manipulating TJ complexes like ethylenediaminetetraacetic acid, chitosan, or poly-L-lysine (PLL), so called TJ modulators, are evolved.[90]

3.2. Benefits of OECTs

The envisioned added value for organic bioelectronics is to replace, where possible, animal models for medical studies. The animal model does not necessarily correctly predict the effect on human tissue, especially regarding neurological diseases such as Alzheimer, epilepsy, or Parkinson. Organic electronics open the possibility to perform experiments using in vitro or even in vivo human tissue culture, such as brain, liver, lung, kidney, and intestine enabling concise investigations on the effects of therapeutics on our body. Organic bioelectronics together with the growing research knowledge on in vitro cell culture of human organ tissue brings hope to overcome the lack of knowledge regarding tumors or infectious diseases due to viruses, like Zika or Covid-19.

The electrical assessing of barrier tissue integrity with the OECT as an impedance sensor was first reported in 2012 by the group of Owens and since then received increasing attention.[61] The sensitivity of OECTs as an impedance sensor can be enhanced through tuning of channel area according for a broad range of tissue resistance. As mentioned before, the sensitivity

of OECTs can be tuned according to the required range of monitored cell barrier resistance.[72,60] After first time monitoring cell layer integrity with the OECT in the group of Owens in 2012, the OECT established as a validated complementary or alternative method for in vitro and future in vivo biomedical applications, for example, monitoring minute changes of tissue under the effect of toxins.[64] Utilizing the OECT supported by imaging methods is state-of-the-art and provides valuable insights to understand monitored results on biosensing.[69,71,98] The group of Owens evolved a fully automated electrical wound-healing assay utilizing OECTs.[69] Taking advantage of the transparent nature of PEDOT:PSS, the healing process has been simultaneously monitored electrically and optically in this project. In comparison to sheer optical techniques, the OECT offers two advantages, monitoring with higher sensitivity and in situ.[69] It monitors conformational changes of integrated cells with higher sensitivity and is even able to detect metabolites. The capability to provide real-time measurements of cell structure broadens the range of possibilities to apply the OECT in in vitro and in vivo research extensively, compared to end-point measurements in case of, for example, immunofluorescence.[69] The ability to customize the transistor configuration and mechanical properties according to the studied tissue structure is outstanding.[57,72,99] Research results, such as the integration of a microfluidic platform,[69] or 3D cardiac tissues[57] show the potential of OECTs for in vitro biosensing. Furthermore, the OECT-based barrier tissue integrity evolved for sensing,[26,60,72,100] controlling and/or monitoring cell growth and tissue formation (**Figure 2a**).[61,64,71,101] TJ opening or irreversible disruption using agents, such as hydrogen peroxide, ethanol, EGTA, Salmonella, and silver nanoparticles, has been monitored by transient response measurements.[55,61,66,67,71,102] Highlighting here the work of Decataldo et al., where the ability of OECTs to assess coating-dependent toxicity of nanoparticles on barrier tissue and non-barrier tissue has been reported.[66] The recent published work of Yeung et al. showed that the OECT is able to in situ monitor cancer invasion and metastasis of NPC43 cells on Caco-2 cells, using a multichannel recording OECT array.[103] Utilizing the OECT as an impedance sensor is crucial in the fields of toxicology, drug delivery, infectious disease diagnostics, and basic research on molecular biology and electrophysiology of barrier tissue.

3.3. Monitoring Barrier Tissue Integrity with the OECT in Standard Configuration

The work of Jimison et al. in 2012 represents a milestone in the field of impedance sensing with OECTs.[61] Sensing the barrier function of tissues in vitro, with an integrated tissue between apical and basal electrolyte is of great importance for toxicological and drug delivery studies. Utilizing a permeable Transwell filter, where cells are seeded on a porous membrane, not only enables an easy transfer, but also mimics in vivo conditions.[61] Besides the TER-value accounting for the ion flux through the tissue (R_{MEM}), the ion accumulation at the barrier tissue interface is expressed by the capacitance C_{MEM} (Figure 2b). Furthermore, the ion flux alters with the apical and basal electrolyte resistance R_{MED}, the resistance and the capacitance of the filter, and the capacitance of the channel C_{CP}. In the well-established standard
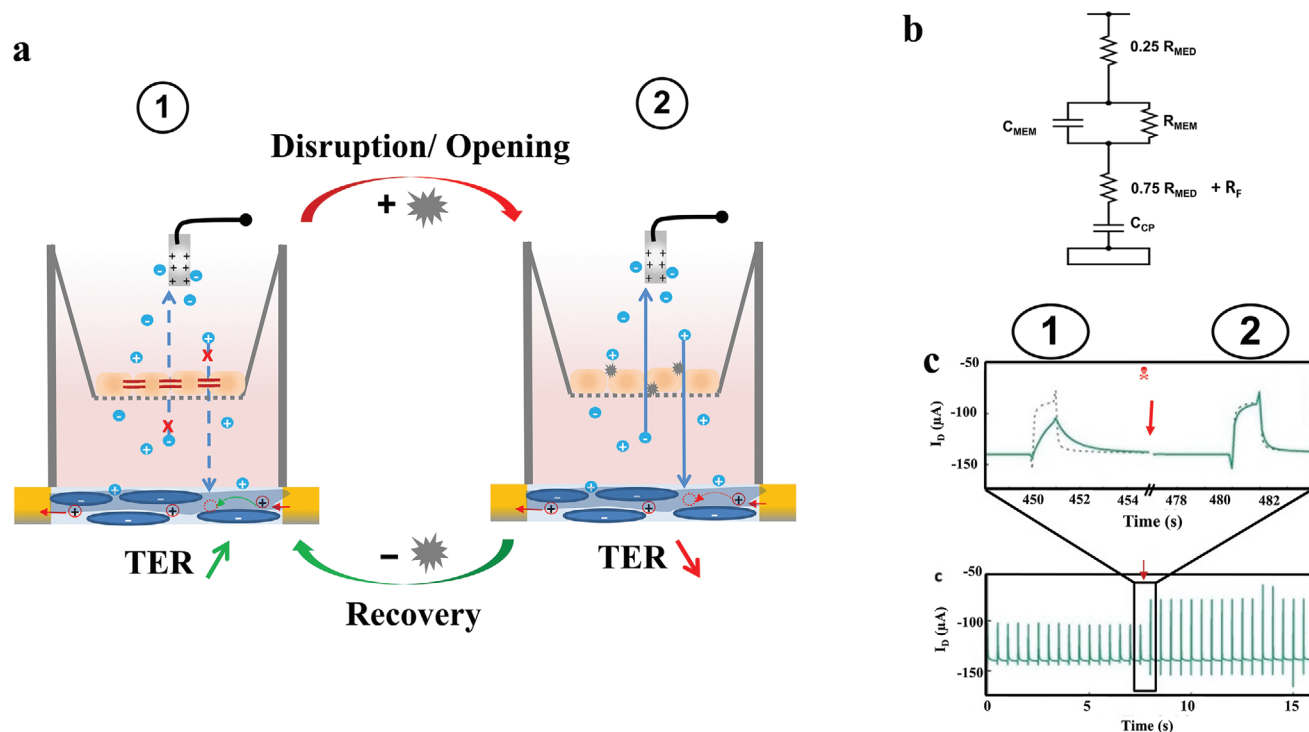
Figure 2. Sensing barrier integrity and barrier disruption with the standard OECT configuration. a) Schematic of the OECT with integrated tissue as an intact barrier functionality due to the presence of tight junctions (TER high, (1) left) and without barrier function due to the loss of tight junctions (TER low, (2) right). The tight junction disruption or opening and recovery is controlled by adding (red arrow) and removing (green arrow) a chemical agent (grey symbol). Reproduced with permission.[108] Copyright 2021, Wiley-VCH GmbH. b) Electronic circuit describing ionic transport between gate electrode and transistor channel. R_{MEM} and C_{MEM} refer to the trans epithelial resistance and the capacitance of the cell layer, respectively. R_F relates to the resistance of the permeable filter. R_{MED} refers to the resistance of the permeable filter and cell culture media. C_{CP} refers to the capacitance of PEDOT:PSS as conducting polymer in the channel. Reproduced with permission.[61] Copyright 2012, Wiley-VCH GmbH. c) Transfer characteristics of the transient response of I_D to a V_G pulse, where $V_G = 0.3$ V was applied for 1 s and off for 29 s, and at a constant $V_D = -0.1$ V. ① Monitoring barrier tissue integrity by measuring the response of I_D (solid line) in contrast to the reference, response of I_D in absence of cells (dashed lines). The red arrow indicates the time H_2O_2 was added. ② Monitoring the disruption of barrier tissue by measuring the response of I_D with an integrated barrier tissue after the addition of 100 mм H_2O_2 (solid lines) in contrast to the reference (dashed lines). Over all, the OECT response was measured in situ for periodic square V_{GS} pulses over 15 min. Reproduced with permission.[61] Copyright 2012, Wiley-VCH GmbH.

OECT configuration, the transient response of I_D is measured at a certain V_D by applying a V_G pulse. Minute variations in the paracellular ion flux into the channel are detected in real time by a change in I_D. Jimison et al. showed, as displayed in Figure 2c, that the OECT reveals a smaller decay in the transient response of I_D in presence of barrier tissue (solid line) as compared to the transient response in absence of barrier tissue (dashed line), where a larger change in I_D was measured (Figure 2c ①).[80] OECTs in standard configuration are able to monitor the barrier disruption due to the exposure to toxins, such as H_2O_2 (100 mм), displayed as an overlap with the electrical characteristics of the filter in absence of cells (Figure 2c ②).

In general, with an increase in permeability the TER-value decreases.[104] The standard OECT configuration displays a sufficiently HS to distinguish the concentration dependent barrier disruption as a change in I_D due to the exposure to a series of H_2O_2 concentrations (100, 50, 5, and 1 mм) in real time (**Figure 3a**). Furthermore, the standard OECT is applicable as a sensitive sensor for milder barrier disruption due to the less toxic compound ethanol (EtOH) for several concentrations (30%, 20%, and 10 %) (Figure 3b). The work benchmarked the transient re-

sponse measurement of I_D using the OECT in standard configuration to assess barrier tissue integrity and barrier disruption in real time and to distinguish concentration-dependent toxicity. Thus, the OECT impedance sensor found its application in evaluating toxicology of chemicals.

4. Enhanced Ion Sensitive Current-Driven OECT Configuration

4.1. High-Sensitive Ion Detection at Low Voltages with Current-Driven OECTs

The OECT in standard configuration is a sensitive method to detect the presence of a barrier tissue. However, state-of-the-art transistor-based approaches have an intrinsic trade-off between sensitivity, ion concentration range, and operating voltage.[105] The current-driven configuration provides a simple yet effective approach overcoming this fundamental limit. **Figure 4a**,b shows the schematic 3D structure and the corresponding circuit of an OECT connected in a current-driven configuration. The current-driven configuration resembles an inverter-topology, where the
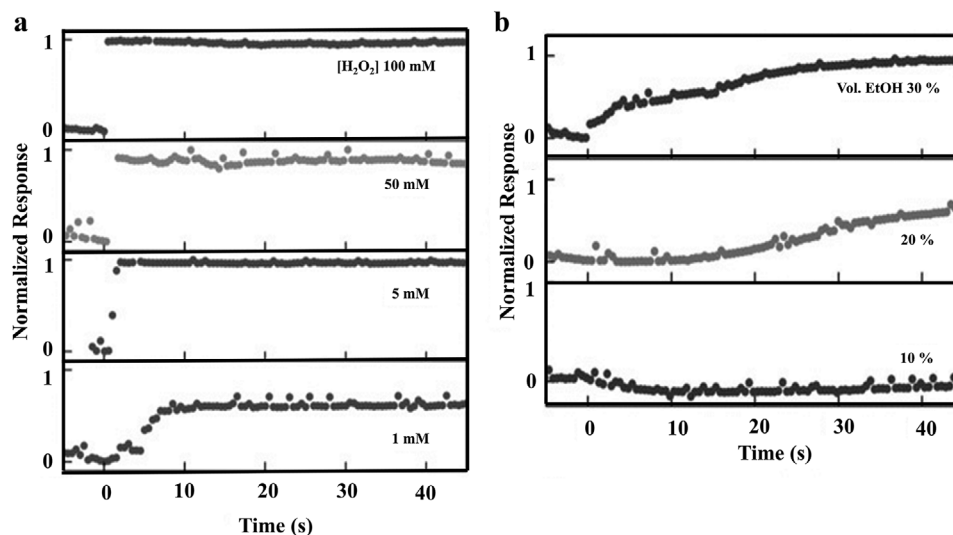
ADVANCED
SCIENCE NEWS

www.advancedsciencenews.com

ADVANCED
HEALTHCARE
MATERIALS

www.advhealthmat.de

Figure 3. Monitoring barrier tissue disruption with the OECT in situ due to the addition of toxins. The normalized response (NR) is obtained by calculating $\Delta I_D / I_O$ (where ΔI_D refers to drain current modulation in response to the application of V_G, and I_O refers to the drain current when V_G is off) and subsequently normalizing the dataset to [0,1]. a) Change in the normalized response (NR) after the addition of H_2O_2 at $t = 0$ s for several concentrations (100, 50, 5, and 1 mм). Here, NR = 0 corresponds to full barrier properties of a confluent monolayer and a NR = 1 corresponds to a cell layer with no barrier properties. Reproduced with permission.[61] Copyright 2012, Wiley-VCH GmbH. b) Change in the NR after the addition of EtOH at $t = 0$ s for volume concentrations of 30%, 20%, and 10 %. Reproduced with permission.[61] Copyright 2012, Wiley-VCH GmbH.
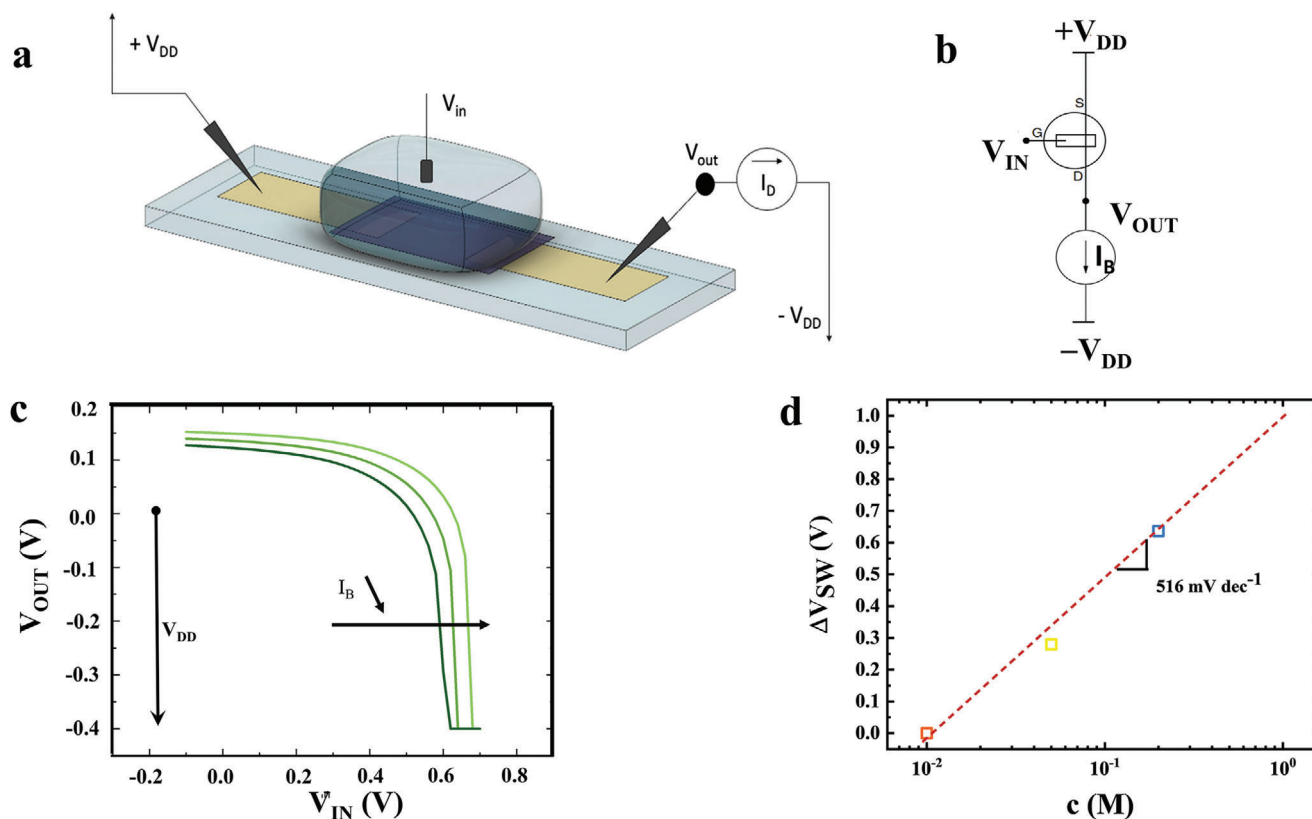

Figure 4. Current-driven OECT used as ion sensor. a) Device architecture of a current-driven OECT configuration. b) Schematic circuit of the OECT in current-driven configuration. c) Measured transfer characteristics of a current-driven OECT for various $I_B = 1.25$, 1.00, and 0.75 mA and $|V_{DD}| = 0.4$ V. The gate is an Ag/AgCl pellet and the OECTs geometries are: $W = 1000$ µm, $L = 2000$ µm, $t = 300$ nm. As electrolyte NaCl (aq) was used in a concentration of 0.1 м. d) Cumulative switching voltage variation $\Delta V_{SWi + 1} = \Delta V_{SWi} + (V_{SWi + 1} - V_{SWi})$ as a function of ion concentration. The average sensitivity calculated by last-square linear approximation is of 516 mV dec^{-1}. The gate electrode is a tungsten foil and the OECTs geometries are: $W = 1000$ µm, $L = 300$ µm, $t = 25$ nm. Reproduced with permission.[106] Copyright 2018, Springer Nature.

**ADVANCED
SCIENCE NEWS**

www.advancedsciencenews.com

**ADVANCED
HEALTHCARE
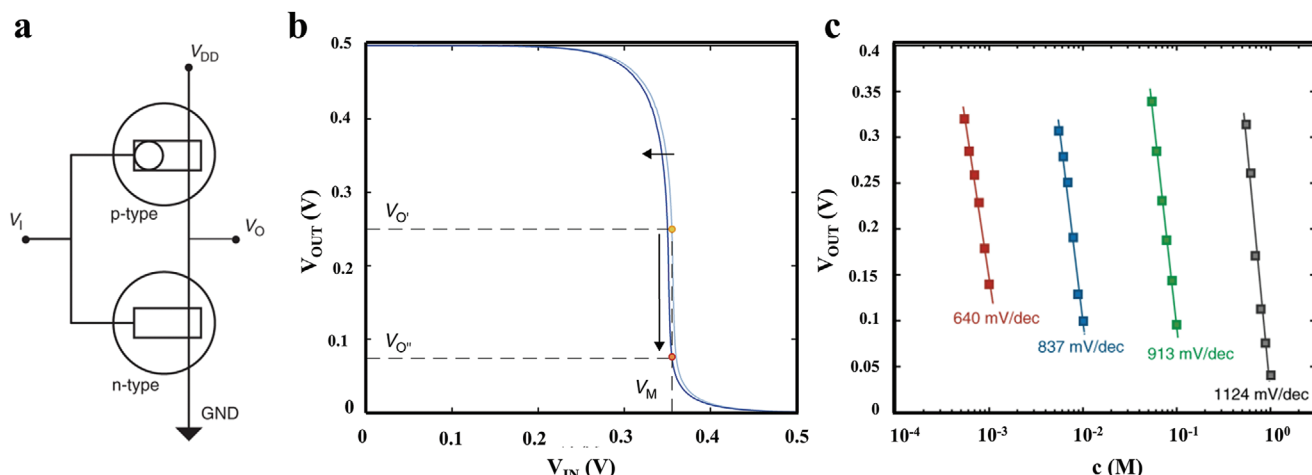MATERIALS**

www.advhealthmat.de

Figure 5. The OECT complementary amplifier. a) Schematic circuit of the OECT complementary amplifier. The V_{IN} is connected to the gates of the transistors, and V_{OUT} is collected at their drains. V_{DD} is connected to the source of the p-type OECT, and the source of the n-type is grounded (GND, $V_{GND} = 0$ V). b) Transfer characteristic of an OECT complementary amplifier. The red dot identifies V_M (i.e., the required V_{IN} to have $V_{OUT} = V_{DD}/2$). To operate the OECT complementary amplifier with high sensitivity, the input voltage is biased at $V_{IN} = V_M$, while the output voltage is continuously measured. Light-blue characteristic: at $V_{IN} = V_M$ the output $V_{OUT} = V_{OUT'}$ and the ion concentration is c_0. A small variation of the ion concentration results in a shift of the electrical characteristic (from light blue to dark-blue) and this, in turn, in a large variation of the output voltage from $V_{OUT'}$ to $V_{OUT''}$. c) Real time high-sensitivity ion detection: Measured V_{OUT} as a function of c in various sub-range of concentrations, covering the whole physiological range. The ion concentration where $V_{OUT} = V_{DD}/2$ is $c_0 = 7.8 \times 10^{-4}$, 7.8×10^{-3}, 7.8×10^{-2}, and 7.8×10^{-1} M. Full lines are the linear least square fit to the measurements, yielding SA. The electrolyte concentration is increased every 30 s. The measurements are performed at $V_M = 0.415$ V. Reproduced with permission.[109] Copyright 2020, Springer Nature.

pull-down transistor is replaced with a current generator (I_B). In this configuration, the source is connected to the supply voltage V_{DD}, the drain is the output voltage V_{OUT}, while the input voltage V_{IN} is applied to the gate ($V_G = V_{IN}$).[106] The $V_{IN} - V_{OUT}$ electrical characteristics of the current-driven OECT configuration can be related to the OECT parameters and current bias I_B as follows:

$$V_{OUT} = V_{DD} - I_B \, r_{channel} \tag{1}$$

The channel resistance depends on the operating region of the OECT. When the current-driven OECT is biased between negative V_{IN} and $V_{IN} = 0$, anions are injected into the CP, the hole concentration in the polymer is increased, and the OECT operates in the linear region. According to the Bernards–Malliaras model[107] the drain current then reads:

$$I_D = k_n \left[(V_T - V_{GS}) V_{SD} + \frac{V_{SD}}{2} \right] \tag{2}$$

where $k_n = W \, t \, C_v \, \mu \, L^{-1}$, W, L, and t are the channel width, length, and thickness, respectively, C_v is the volumetric capacitance and μ and the mobility. In the current driven configuration $V_{GS} = V_{IN} - V_{DD}$, $V_{SD} = V_{DD} - V_{OUT}$ and the OECT channel resistance results:

$$r_{channel(lin)} \cong \frac{1}{k_n (V_{DD} + V_T - V_{IN})} \tag{3}$$

Combining Equations (1) and (3) results:

$$V_{OUT} = V_{DD} - \frac{I_B}{k_n (V_{DD} + V_T - V_{IN})} \tag{4}$$

Equation (4) shows that when V_{OUT} depends on the supply voltage V_{DD}, on the bias current I_B, on the input voltage V_{IN}, and the OECT parameters k_n and V_T. In the current driven configuration I_B is a design variable that enables the low-voltage operation independently of the ion concentration of the electrolyte, as displayed in Figure 4c, and/or the specific biological properties of the cell layer.[81,108,109] When V_{IN} is small, the OECT channel resistance is small and $V_{OUT} \approx V_{DD}$. Equation (4) also shows that V_{OUT} decreases by increasing V_{IN}. When $V_{OUT} < V_{IN} - V_T$ the OECT operates in saturation region and the drain current reads:[107]

$$I_D = k_n \, (V_T - V_{GS}) (1 + \lambda V_{SD}) \tag{5}$$

where λ is the channel length modulation. When the OECT operates in saturation, its output resistance is large since it behaves like a current generator and hence V_{SD} is large. Combining Equation (1) with (5) and considering the current-driven topology, the output voltage reads:

$$V_{OUT} \approx V_{DD} - \frac{I_B}{\lambda k_n (V_{DD} - V_{IN} + V_T)^2} \tag{6}$$

We note that in the case of OECTs λ is typically smaller than 10^{-3} V^{-1} and this explain the large variation of V_{OUT} when V_{IN} is closed to the switching voltage V_{SW}. Indeed, when the OECT is operating in salutation region, the current-driven OECT operates as a common-source amplifier and its voltage gain $\delta V_{OUT}/\delta V_{IN} = g_m \, r_{channel(sat)}$ which corresponds to the intrinsic gain of the transistor.[110]

The figure of merit of a current-driven OECT is the switching voltage V_{SW}. Previous work focused on ion detection with a current-driven OECT demonstrated a sensitivity of up to

**ADVANCED
SCIENCE NEWS**
www.advancedsciencenews.com

**ADVANCED
HEALTHCARE
MATERIALS**
www.advhealthmat.de

$\Delta V_{SW}/\Delta c$ = 516 mV dec^{-1}, extracted from measured transfer characteristics at various NaCl concentrations, as shown in Figure 4d. This was more than one order of magnitude larger than the Nernst limit, also exceeding the sensitivity of several state-of-the-art ion-sensitive transistors, including Si ISFETs, ZnO FETs, a-IGZO double gate FETs, Si nanowire FETs, graphene FETs, EGOFETs, and OECTs in standard configuration. To fairly compare the various technologies, the sensitivity is normalized to the supply voltage V_{DD}. The comparison shows that the current-driven configuration provides the best performance because it has the advantage of combining low-voltage operation with high ion sensitivity. Moreover, when combined with an ion-selective membrane (ISM), the OECT current-driven configuration achieved a sensitivity of 414 mV dec^{-1}, which is close to the value obtained in absence of the ISM. The ISM is implemented between the analyte and the inner electrolyte on the channel.[111] Thus, the current-driven OECT configuration can also operate with HS as an ion selective sensor. The reproducibility of the platform depends on the stability of the deposited PEDOT:PSS polymer and on the amount of fixed charges into the polyelectrolyte (PSS) phase.[112] The stability of the polymer on glass is maximized by using GOPS in the PEDOT:PSS formulation.[112] The amount of fixed charges into the polyelectrolyte (N_{fix}) depends on the polymer formulation and in the case of PEDOT:PSS results in $N_{fix} = 10^{21}$ cm^{-3}, that is, 1.66 м. As a result, when the ion concentration is smaller than about 1 м, the OECT threshold voltage increases (i.e., becomes more negative), the shift amounts to 112 mV per decade of ion concentration decrease (dec). We verified that this result is very reproducible, which has a variability of only about 1 mV dec^{-1}. The results in Figure 4d do not include error bars. However, during the last years we mainly focused on the current-driven architecture for monitoring cell layers.[108] Furthermore, we further developed high-sensitivity ion-detection and monitoring with the complementary OECT amplifier architecture.[109] Overall, the various experiments provided an excellent reproducibility and stability of these architectures for both ion sensing and cell monitoring.

4.2. Complementary OECT Amplifier Based on the Current-Driven OECT Architecture

Recently, Romele et al. has extended the current-driven architecture by substituting the current generator with an n-type OECT.[109] This new architecture, named complementary OECT amplifier, is the very same topology of a complementary inverter but it is operated in analogue fashion, exploiting the circuit amplification. The schematic circuit diagram is displayed in **Figure 5a**. The input voltage V_{IN} is applied at the gates of the transistors and V_{OUT} is collected at their drains. In this configuration V_{DD} is applied at the source of the p-type OECT whereas the source of the n-type OECT is grounded. There are two modes of operation of the OECT amplifier. The wide-range (WR) mode is analogous to the current-driven operation. V_I is swept from GND (0V) to V_{DD} and V_{OUT} is recorded. The transition voltage, defined as the V_I such that $V_{OUT} = V_{DD}/2$ is analogous to the V_{SW} in the current-driven configuration and depends on the ion concentration in the electrolyte. When operated in WR mode, the

OECT amplifier takes advantage of a relatively low ion sensitivity to span the physiological range of ion concentration with a supply voltage as low as 0.5 V. Therefore, the WR mode enables to quantify the initial analyte concentration spanning several orders of magnitudes. Then, in order to detect small variations from the background concentration, a HS is required.

The HS mode of operation is schematically illustrated in Figure 5b. After using the OECT ion-sensitive amplifier in WR mode, the extracted $V_{O'}$ yields the initial background ion concentration. To operate in the HS mode, the input voltage is then set to V_I such that $V_{OUT} = V_{O'}$. In this working region the output voltage is extremely sensitive to a shift in the transfer characteristic (i.e., dV_{OUT}/dV_I is large), and a small variation of ion concentration results in a large variation of V_{OUT} from $V_{O'}$ to $V_{O''}$ (from light blue to dark-blue, Figure 5b). The sensitivity of the OECT complementary amplifier is tunable by the design parameters, transconductance, and channel length modulation of the p- and n-type transistors during fabrication,[107] but also by V_{DD}, which enables fine-tuning. With an increase in V_{DD} from 0.4 to 0.5 V, the sensitivity almost doubled from 480 to 910 mV dec^{-1}.

By integrating an ISM, such as a K$^+$-selective membrane, the OECT complementary amplifier operates as an ion selective sensor without losing sensitivity, as shown for K$^+$ concentrations in a range of 10^{-4}–1 м (Figure 5c). The circuit-oriented device-aware sensor design approach enables the OECT complementary amplifier to operate with a top performing wide range and unprecedented sensitivity larger than 2300 mV V^{-1} dec^{-1}, combined with real-time operation, tunable performances, and low operating supply voltage. It provides both ion detection over an ion concentration range of five orders of magnitude and real-time monitoring of variations two orders of magnitude lower than the detected concentration. The HS, multiscale, and reconfigurable operation provided by the OECT complementary amplifier can be extremely relevant also in the emerging research field of bioelectronic sensors to improve the signal-to-noise ratio, resolution, and robustness.[113]

5. Current-Driven OECT to Study Barrier Tissue

5.1. Sensing Irreversible Barrier Tissue Disruption

When monitoring small changes in the TER of barrier tissue, after adding a toxin in low concentration, a highly ion-sensitive impedance sensor is required. Due to the high ion sensitivity and low operating voltage, the OECT in current-driven configuration is a promising approach to sense barrier tissue integrity. A proven advantage of the current-driven OECT configuration is the possibility of tuning the operating range and voltages by means of the bias current I_B. This is very important when applied in bioelectronics, because the operation in an appropriate voltage window can limit possible side redox reactions that can be harmful for the biology. Here, the ion-sensitivity of OECTs, using similar channel geometries, in current-driven configuration is compared to the standard configuration used by Jimison et al. in 2012, studying the effect of toxins, such as H$_2$O$_2$, on the barrier function of Caco-2 cells.[61] Barrier tissue disruption 60 min after adding 5 mм H$_2$O$_2$ has been monitored using the OECT in current-driven configuration (**Figure 6a**) and in standard configuration (Figure 6b).[81] However, when comparing the response
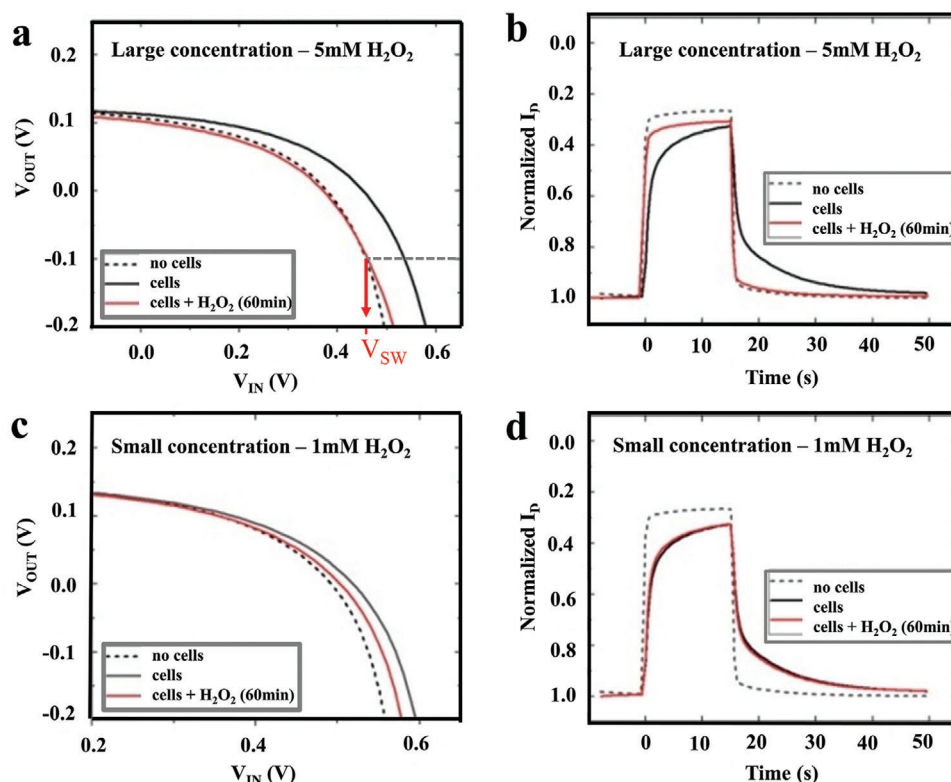
Figure 6. Sensing cell barrier integrity for H_2O_2 with an OECT in current-driven configuration. The OECT response in the absence and presence of barrier tissue adding a,b) 5 mM H_2O_2 and c,d) 1 mM H_2O_2 in the current-driven (a,c), and in the standard configuration (b,d). The transfer characteristics were taken at $V_{DD} = 0.2$ V and $I_B = -1.1$ mA (a) and -0.6 mA (c) in the current-driven configuration. In the standard configuration $V_D = -0.1$ V was used. Device dimension were $W = 2$ mm, $L = 1$ mm, $t = 100$ nm. An Ag/AgCl gate electrode and EMEM cell culture medium as an electrolyte was used. Reproduced with permission.[81] Copyright 2019, Wiley-VCH GmbH.

over time the enhanced ion-sensitivity of current-driven OECTs is evident. Extracting the response of the OECT is more evident in the current-driven configuration, where it is directly revealed in the graph as the shift of V_{IN}, whereas in standard configuration an exponential fit of I_D has to be performed. Hence, operating the OECT in current-driven configuration monitors barrier disruption over time with higher sensitivity. The experiment has been repeated for a smaller concentration of 1 mM H_2O_2. The minor disruption of barrier function could only be monitored with the current-driven configuration (Figure 6c), but not with the reference method (Figure 6d). The enhanced sensitivity of the OECT, when operating in current-driven configuration, confirms the validity of using the OECT as biosensor in current-driven configuration.

5.2. Sensing Reversible Barrier Tissue Modulation

As next step, the current-driven OECT with integrated barrier tissue was used to sense the reversible loss of barrier function. Besides toxicological studies, the effect of TJ modulators, which cause temporal opening of TJs without an irreversible barrier disruption, is of great importance. TJ opening and therefore a decay of barrier function is in accordance with an increase of ion permeability. Once the modulator is removed, TJs form again and

a recovery of barrier function in accordance with a decrease in ion permeability is enabled.[82,84,114] As a controlled TJ modulation is crucial for an oral intake of drugs through organs into our blood,[87] sensing TJ modulation with non-invasive methods is of great importance for drug delivery. The amino acid-based polycation PLL is well-studied to modulate TJs and commercially available.[115] Polycations, like chitosan or PLL, are potential TJ modulators across intestinal barrier tissues.[116] Polycations represent the most convenient manner to affect oral bioavailability having attributes such as enhancing drug solubility, protecting sensitive drugs from rapid degradation due to positive charges at a broad pH range, and serving as TJ modulator.[117] Furthermore, it has been demonstrated that PLL induces reversible TJ modulation through morphological modifications of the F-actin cytoskeleton as well as a redistribution of zonulin and occludin.[19] Therefore, recording temporal TJ modulation under the influence of a polycationic modulator is of great importance to assess the transient state of barrier functionality with potential applications in drug delivery. Recently, Lieberth et al. have demonstrated the current-driven OECT as a suitable biosensor for impedance modulation of barrier tissue.[108] More in detail, the current-driven OECT was used to monitor in situ the temporal barrier modulation and recovery, using Caco-2 barrier tissues under the effect of PLL as a case study (**Figure 7a**). To evaluate the device characteristics, V_{IN} was applied to the device with an integrated
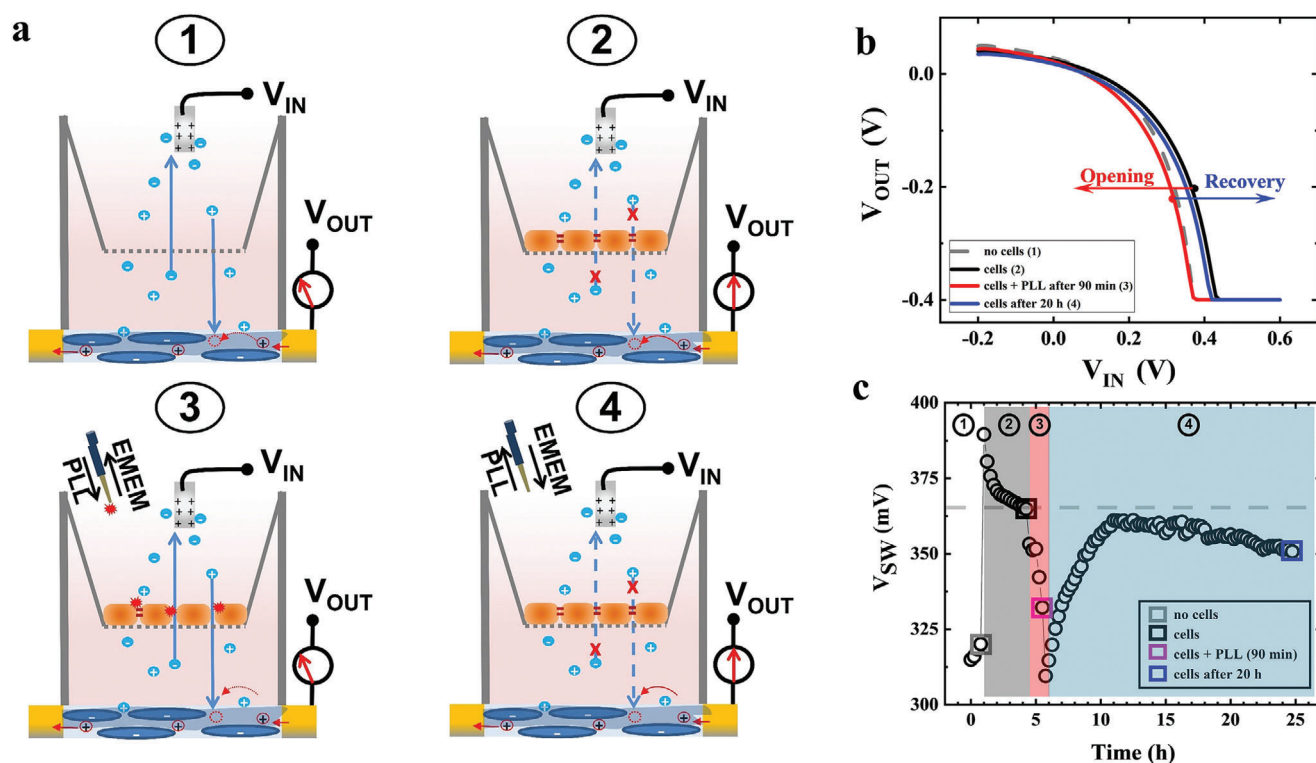
2100845 (10 of 16)

Figure 7. Sensing reversible tight junction modulation over time with a current-driven OECT: a) Schematic of the four experimental steps performed under physiological conditions: The device with an integrated Transwell filter in 1) absence and in 2) presence of a Caco-2 cell layer; The barrier functionality of the integrated cell layer is symbolized by TJs (red). 3) Addition of PLL, while keeping the electrolyte volume constant; 4) incubation after exchanging electrolyte apical and basal. b) Detecting (V_{OUT}–V_{IN})-transfer characteristics of a current-driven OECT at $I_B = 0.5$ mA and $V_{DD} = -0.4$ V under physiological conditions. Selected (V_{OUT}–V_{IN})-transfer characteristics of the OECT in absence (grey dashed, 1) and presence (black, 2) of the barrier tissue, 90 min after adding PLL (red, 3) and 20 h after exchanging the electrolyte (blue, 4). c) Monitoring the extracted V_{SW} of all measured (V_{OUT}–V_{IN})-transfer characteristics over time of the experiment. The OECT's geometries were $W = 2$ mm, $L = 1$ mm, $t = 100$ nm. Ag/AgCl was utilized as gate electrode and EMEM as an electrolyte. For this experiment Caco-2 cells were seeded on a Transwell filter (1.12 cm^2, pore size: 0.4 μm) and measured on day 14. Reproduced with permission.[108] Copyright 2021, Wiley-VCH GmbH.

Transwell filter only (1), so that cations from the electrolyte were not facing barrier tissue. Then an intact barrier tissue was introduced as reference, the ion permeability between the apical and basal compartment is impeded by TJs (2). Upon addition of 162 μ PLL on the apical side, the TJs open and the ion flow is restored after 90 min (3). After the extraction of PLL by exchanging the electrolyte and further incubation time, the TJs recovered and an intact barrier tissue is regained (4). Due to its HS, the current-driven OECT enabled the in situ monitoring of reversible TJ modulations as a variation of V_{OUT} (Figure 7b). Upon the addition of 162 μ PLL on the apical side, a systematic shift of electrical characteristics toward smaller V_{IN} (3, red) was recorded and the corresponding decay of V_{SW} indicates TJ opening. Overlapping with the electrical characteristics of the device in absence of barrier tissue, labeled as "no cells" (1, grey), electrical characteristic after PLL exposure (3, red) demonstrates a complete loss of barrier function. After the extraction of the TJ modulator, a back-shift of electrical characteristics (4, blue) indicates a recovery of the barrier function. A full recovery of TJs was detected after 12 h, when the electrical characteristics of (4) and (2) overlap. Due to the low operating voltage, the current-driven OECT successfully operates in real time over an extended time scale of 24 h (Figure 7c). V_{SW}, extracted at $V_{OUT} = V_{DD}/2$, portrays minor changes of the trans-

fer characteristics V_{OUT}–V_{IN} during TJ modulation as a function of time.

By monitoring the effect for three different PLL concentrations, 81 (small), 162 (medium), 324 μ (high), the application of the current-driven OECT shows HS for impedance sensing (**Figure 8a**). The exposure to a low PLL concentration (3, red) resulted in a small change in V_{SW}, as the barrier function decreased only slightly. After the exchange of electrolyte (4, blue), V_{SW} increases overcoming the level of the intact barrier tissue. Hence, a low PLL concentration had no effect on TJ modulation. The effect was far more pronounced in case of adding a medium PLL concentration, causing reversible TJ modulation. When adding a high PLL concentration, V_{SW} decreased directly to the reference response in absence of barrier tissue and remained constant during and after the exposure and therefore causes an irreversible alteration of barrier properties. The recovery of TJs is rather slow, as it requires the transport of occludin and zonulin from the inner of the cell to the membrane. As a complementary method optical visualization with confocal laser scanning microscopy (Figure 8b) was performed, when immunocytochemically staining the TJ protein occludin, to highlight the effect on the TJ barrier integrity after PLL exposure (3), and after an incubation time subsequent to PLL exposure (4). Images after 90 min of PLL exposure
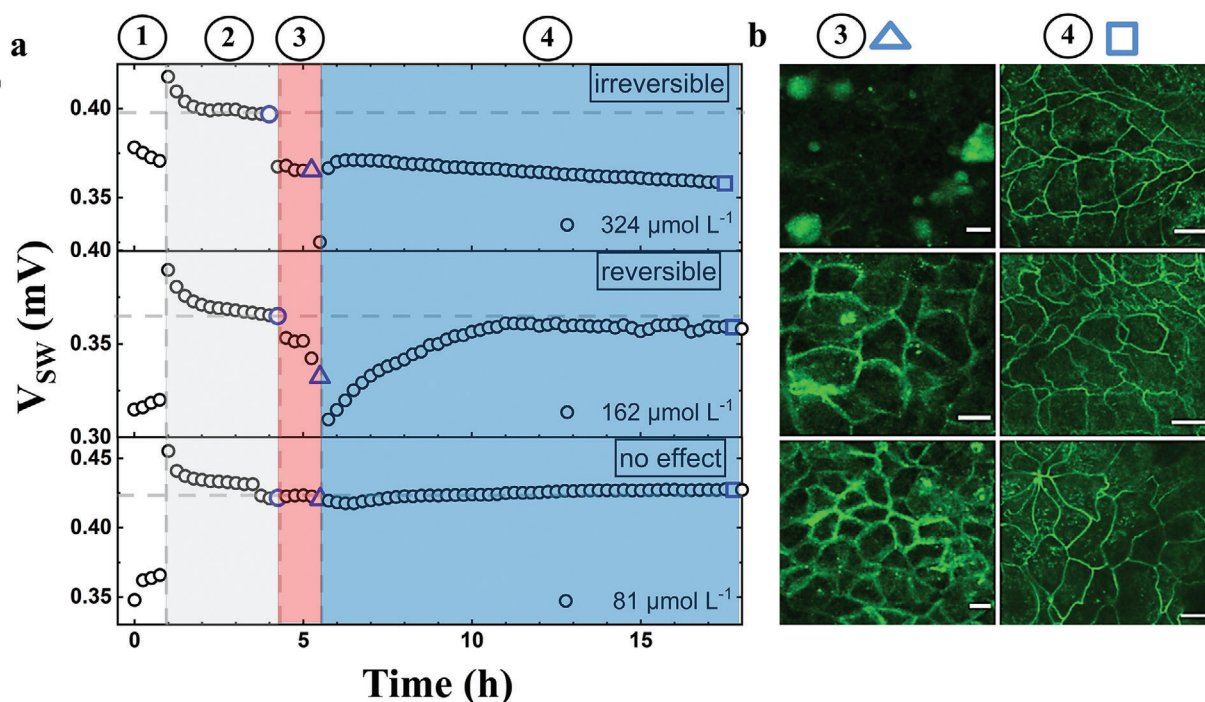
**ADVANCED
SCIENCE NEWS**

www.advancedsciencenews.com

**ADVANCED
HEALTHCARE
MATERIALS**

www.advhealthmat.de

Figure 8. a) V_{SW} over time of the experiment for three different concentrations of PLL (81, 162, and 324 μ). Vertical grey lines help to distinguish experimental steps. Horizontal grey dashed lines indicate V_{SW} of intact barrier tissue. b) Immunostaining of occludin (green) in human CaCo-2 cells cultivated on day 14 on coverslips (1.12 cm^2) and treated with different amounts of PLL (directly after 90 min of exposure (Δ) and after 20 h of recovery (□). All scale bars represent 10 μm. Reproduced with permission.[108] Copyright 2021, Wiley-VCH GmbH.

for low and medium PLL concentration show a similar staining pattern compared to the untreated barrier tissue. Only the occludin staining for high PLL concentration is clearly impaired. The temporal loss of barrier function due to a medium PLL concentration, monitored with the current-driven OECT is not visible in the occludin staining due to limits in the optical resolution compared to the size of TJs. Images taken after exchange of the electrolyte and an incubation time project an intact occludin pattern for all three PLL concentrations. In conclusion, combining the results of both techniques for a high PLL concentration, occludin proteins are steadily resembled during the time of recovery at the outer cell membranes, but lost their barrier function, firmly sealing all junctional cell connections. This confirms once more the power of the highly sensitive current-driven OECT as a valid impedance sensor for barrier tissue. This work shows the progress of OECT technology toward in vitro testing of TJs for clinical applications, such as drug targeting and screening.

6. Conclusion

In this progress report, the promising potential of OECTs in current-driven configuration for in vitro monitoring of barrier tissues is discussed, crucial for toxicological characterization of chemical compounds and drug delivery. The current-driven OECT offers a record ion-sensitivity at low operating voltage, exceeding the Nernst limit by one order of magnitude. The enhanced ion-sensitivity is demonstrated by measuring the irreversible disruption of barrier tissue, such as epithelial Caco-2 cell layer, on the addition of toxins as H_2O_2. Furthermore, the recent

achievements in measuring TJ modulation, impeding the transcellular pathway in barrier tissue of nutrients and drugs, are described. The progress to in situ monitor reversible opening and closing of TJs under the effect of drug additives, such as PLL, is highlighted. The fast development of the OECT as impedance sensor over the past ten years gives promising perspectives for a broad range of applications.

Conflict of Interest

The authors declare no conflict of interest.

[1] M. Prentki, T. J. Biden, D. Janjic, R. F. Irvine, M. J. Berridge, C. B. Wollheim, *Nature* **1984**, *309*, 562.

[2] A. Carlsson, *Adv. Neurol.* **1993**, *60*, 1.

[3] J. D. Watson, F. H. C. Crick, *Nature* **1953**, *171*, 737.

[4] L. Pauling, C. Niemann, *J. Am. Chem. Soc.* **1939**, *61*, 1860.

[5] M. Ramuz, A. Hama, M. Huerta, J. Rivnay, P. Leleux, R. M. Owens, *Adv. Mater.* **2014**, *26*, 7083.

[6] S. Tria, L. H. Jimison, A. Hama, M. Bongo, R. M. Owens, *Biosensors* **2013**, *3*, 44.

[7] a) J. P. Giraldo, M. P. Landry, S. M. Faltermeier, T. P. McNicholas, N. M. Iverson, A. A. Boghossian, N. F. Reuel, A. J. Hilmer, F. Sen, J. A. Brew, M. S Strano, *Nat. Mater.* **2014**, *13*, 400; b) E. Stavrinidou, R. Gabrielsson, E. Gomez, X. Crispin, O. Nilsson, D. T. Simon, M. Berggren, *Sci. Adv.* **2015**, *1*, e1501136.

[8] a) D. R. Lovley, *Annu. Rev. Microbiol.* **2012**, *66*, 391; b) A. Operamolla, R. Ragni, F. Milano, R. R. Tangorra, A. Antonucci, A. Agostiano, M. Trotta, G. Farinola, *J. Mater. Chem. C* **2015**, *3*, 6471.

[9] D. T. Simon, E. O. Gabrielsson, K. Tybrandt, M. Berggren, *Chem. Rev.* **2016**, *116*, 13009.

[10] a) J. Y. Wong, R. Langer, D. E. Ingber, *Proc. Natl. Acad. Sci. USA* **1994**, *91*, 3201; b) C. E. Schmidt, V. R. Shastri, J. P. Vacanti, R. Langer, *Proc. Natl. Acad. Sci. U. S. A.* **1997**, *94*, 8948.

[11] X. Y. Cui, J. F. Hetke, J. A. Wiler, D. J. Anderson, D. C. Martin, *Sens. Actuators, A* **2001**, *93*, 8.

[12] X. Y. Cui, V. A. Lee, Y. Raphael, J. A. Wiler, J. F. Hetke, D. J. Anderson, D. C. Martin, *J. Biomed. Mater. Res.* **2001**, *56*, 261.

[13] a) D. H. Kim, M. Abidian, D. C. Martin, *J. Biomed. Mater. Res.* **2004**, *71A*, 577; b) T. Nyberg, O. Inganas, H. Jerregard, *Biomed. Microdevices* **2002**, *4*, 43.

[14] X. Cui, D. C. Martin, *Sens. Actuators, B* **2003**, *89*, 92.

[15] M. Asplund, H. von Holst, O. Inganas, *Biointerphases* **2008**, *3*, 83.

[16] C. Weidlich, K. M. Mangold, K. Juttner, *Electrochim. Acta* **2005**, *50*, 1547.

[17] J. Xia, N. Masaki, K. J. Jiang, S. Yanagida, *J. Mater. Chem.* **2007**, *17*, 2845.

[18] a) G. Heywang, F. Jonas, *Adv. Mater.* **1992**, *4*, 116; b) L. Groenendaal, F. Jonas, D. Freitag, H. Pielartzik, J. R. Reynolds, *Adv. Mater.* **2000**, *12*, 481.

[19] J. Rivnay, P. Leleux, M. Sessolo, D. Khodagholy, T. Hervé, M. Fiocchi, G. G. Malliaras, *Adv. Mater.* **2013**, *25*, 7010.

[20] A. Malti, J. Edberg, H. Granberg, Z. U. Khan, J. W. Andreasen, X. J. Liu, D. Zhao, H. Zhang, Y. L. Yao, W. Brill, I. Engquist, M. Fahlman, L. Wågberg, X. Crispin, M. Berggren, *Adv. Sci.* **2016**, *3*, 1500305.

[21] a) G. C. Li, P. G. Pickup, *Phys. Chem. Chem. Phys.* **2000**, *2*, 1255; b) J. Bobacka, A. Lewenstam, A. Ivaska, *J. Electroanal. Chem.* **2000**, *489*, 17.

[22] D. Khodagholy, T. Doublet, P. Quilichini, M. Gurfinkel, P. Leleux, A. Ghestem, E. Ismailova, T. Hervé, S. Sanaur, C. Bernard, G. G. Malliaras, *Nat. Commun.* **2013**, *4*, 1575.

[23] J. Rivnay, P. Leleux, M. F. Ferro, M. Sessolo, A. Williamson, D. Koutsouras, D. Khodagholy, M. Ramuz, X. Stakosas, R. M. Owens, C. Benar, J.-M. Badier, C. Bernard, G. G. Malliaras, *Sci. Adv.* **2015**, *1*, e1400251.

[24] N. K. Guimard, N. Gomez, C. E. Schmidt, *Prog. Polym. Sci.* **2007**, *32*, 876.

[25] a) J. Isaksson, P. Kjäll, D. Nilsson, N. D. Robinson, M. Berggren, A. Richter-Dahlfors, *Nat. Mater.* **2007**, *6*, 673; b) A. Williamson, J. Rivnay, L. Kergoat, A. Jonsson, S. Inal, I. Uguz, M. F. Ferro, A. Ivanov, T. A. Sjöström, D. T. Simon, M. Berggren, G. G. Malliaras, C. Bernard, *Adv. Mater.* **2015**, *27*, 3138; c) D. T. Simon, S. Kurup, K. C. Larsson, R. Hori, K. Tybrandt, M. Goiny, E. W. H. Jager, M. Berggren, B. Canlon, A. Richter-Dahlfors, *Nat. Mater.* **2009**, *8*, 742.

[26] A. Jonsson, Z. Song, D. Nilsson, B. A. Meyerson, D. T. Simon, B. Linderoth, M. Berggren, *Sci. Adv.* **2015**, *1*, 1500039.

[27] J. Y. Kim, J. H. Jung, D. E. Lee, J. Joo, *Synth. Met.* **2002**, *126*, 311.

[28] H. Shi, C. Liu, Q. Jiang, J. Xu, *Adv. Electron. Mater.* **2015**, *1*, 1500017.

[29] L. Kergoat, B. Piro, D. T. Simon, M. C. Pham, V. Noël, M. Berggren, *Adv. Mater.* **2014**, *26*, 5658.

[30] a) E. Stavrinidou, P. Leleux, H. Rajaona, D. Khodagholy, J. Rivnay, M. Lindau, S. Sanaur, G. G. Malliaras, *Adv. Mater.* **2013**, *25*, 4488; b) O. Berezhetska, B. Liberelle, G. De Crescenzo, F. Cicoira, *J. Mater. Chem. B* **2015**, *3*, 5087.

[31] J. Rivnay, S. Inal, A. Salleo, R. M. Owens, M. Berggren, G. G. Malliaras, *Nat. Rev. Mater.* **2018**, *3*, 99.

[32] a) E. Zeglio, O. Inganäs, *Adv. Mater.* **2018**, *30*, e1800941; b) E. Zeglio, M. Vagin, C. Musumeci, F. N. Ajjan, R. Gabrielsson, X. T. Trinh, N. T. Son, A. Maziz, N. Solin, O. Inganäs, *Chem. Mater.* **2015**, *27*, 6385; c) S. Inal, J. Rivnay, P. Leleux, M. Ferro, M. Ramuz, J. C. Brendel, M. M. Schmidt, M. Thelakkat, G. G. Malliaras, *Adv. Mater.* **2014**, *26*, 7450; d) A. Giovannitti, C. B. Nielsen, D.-T. Sbircea, S. Inal, M. Donahue, M. R. Niazi, D. A. Hanifi, A. Amassian, G. G. Malliaras, J. Rivnay, I. McCulloch, *Nat. Commun.* **2016**, *7*, 13066; e) H. Sun, M. Vagin, S. Wang, X. Crispin, R. Forchheimer, M. Berggren, S. Fabiano, *Adv. Mater.* **2018**, *30*, 1704916.

[33] Y. Wen, J. Xu, *J. Polym. Sci., Part A: Polym. Chem.* **2017**, *55*, 1121.

[34] a) H. Shi, C. Liu, Q. Jiang, J. Xu, *Adv. Funct. Mater.* **2015**, *1*, 1500017; b) P. Tehrani, L.-O. Hennerdal, A. L. Dyer, J. R. Reynolds, M. Berggens, *J. Mater. Chem.* **2009**, *19*, 1799; c) Q. Pei, G. Zuccarello, M. Ahlskog, O. Inganäs, *Polymers* **1994**, *35*, 1347; d) ACREO, https://www.acreo.se/expertise/printed-electronic-technologies Accessed February 2021

[35] a) J. F. Franco-Gonzalez, N. Rolland, I. V. Zozoulenko, *ACS Appl. Mater. Interfaces* **2018**, *10*, 29115; b) N. Rolland, J. F. Franco-Gonzalez, R. Volpi, M. Linares, I. V. Zozoulenko, *Phys. Rev. Mater.* **2018**, *2*, 45605.

[36] M. Modarresi, J. F. Franco-Gonzalez, I. Zozoulenko, *Phys. Chem. Chem. Phys.* **2018**, *20*, 17188.

[37] K. Tybrandt, I. V. Zozoulenko, M. Berggren, *Sci. Adv.* **2017**, *3*, eaao3659.

[38] M. Cai, Z. Ye, T. Xiao, R. Liu, Y. Chen, R. W. Mayer, R. Biswas, *Adv. Mater.* **2012**, *24*, 4337.

[39] N. Stutzmann, R. H. Friend, H. Sirringhaus, *Sci. Adv.* **2003**, *299*, 1881.

[40] K. Sun, S. Zhang, P. Li, Y. Xia, X. Zhang, D. Du, F. H. Isikgor, J. Ouyang, *J. Mater. Sci.: Mater. Electron.* **2015**, *26*, 4438.

[41] D. R. Merrill, M. Bikson, J. G. R. Jefferys, *J. Neurosci. Methods* **2005**, *141*, 171.

[42] M. Asplund, T. Nyberg, O. Inganas, *Polym. Chem.* **2010**, *1*, 1374.

[43] C. J. Bettinger, M. Ecker, T. D. Yoshida Kozai, G. G. Malliaras, W. Voit, *MRS Bull.* **2020**, *45*, 655.

[44] A. Tsumura, H. Koezuka, T. Ando, *Appl. Phys. Lett.* **1986**, *49*, 1210.

[45] A. Laiho, L. Herlogsson, R. Forchheimer, X. Crispin, M. Berggren, *Proc. Natl. Acad. Sci. U. S. A.* **2011**, *108*, 15069.

[46] a) Z. T. Zhu, J. T. Mason, R. Dieckmann, G. G. Malliaras, *Appl. Phys. Lett.* **2002**, *81*, 4643; b) L. Torsi, A. Dodabalapur, N. Cioffi, L. Sabbatini, Zambonin, *Sens. Actuators, B* **2001**, *77*, 7; c) D. Li, E. J. Borkent, R. Nortrup, H. Moon, H. Katz, Z. Bao, *Appl. Phys. Lett.* **2005**, *86*, 042105.

[47] C. Bartic, B. Palan, A. Campitelli, G. Borghs, *Sens. Actuators, B* **2002**, *83*, 115.

[48] L. Kergoat, B. Piro, M. Berggren, M. Pham, A. Yassar, G. Horowitz, *Org. Electron.* **2012**, *13*, 1.

[49] F. Buth, A. Donner, M. Stutzmann, J. A. Garrido, *Proc. SPIE* **2012**, *8479*, 84790M.

[50] S. Casalini, F. Leonardi, T. Cramer, F. Biscarini, *Org. Electron.* **2013**, *14*, 156.

[51] A. Loi, I. Manunza, A. Bonfiglio, *Appl. Phys. Lett.* **2005**, *86*, 103512.

[52] a) S. Cotrone, M. Ambrico, H. Toss, M. D. Angione, M. Magliulo, A. Mallardi, M. Berggren, G. Palazzo, G. Horowitz, T. Ligonzo, L. Torsi, et al., *Org. Electron.* **2012**, *13*, 638; b) K. S. Narayan, B. N.

**ADVANCED
SCIENCE NEWS**

www.advancedsciencenews.com

**ADVANCED
HEALTHCARE
MATERIALS**

www.advhealthmat.de

Madhushankar, V. Gautam, S. P. Senanayak, R. Shivanna, *IEEE Electron Device Lett.* **2013**, *34*, 310; c) T. Someya, H. E. Katz, A. Gelperin, A. J. Lovinger, A. Dodabalapur, *Appl. Phys. Lett.* **2002**, *81*, 3079.

[53] a) E. W. Paul, A. J. Ricco, M. S. Wrighton, *J. Phys. Chem.* **1985**, *89*, 1441; b) X. Strakosas, M. Bongo, R. M. Owens, *J. Appl. Polym. Sci.* **2015**, *132*, 41735.

[54] D. Nilsson, T. Kugler, P. O. Svensson, M. Berggren, *Sens. Actuators, B* **2002**, *86*, 193.

[55] S. A. Tria, M. Ramuz, M. Huerta, P. Leleux, J. Rivnay, L. H. Jimison, A. Hama, G. G. Malliaras, R. M. Owens, *Adv. Healthcare Mater.* **2014**, *3*, 1053.

[56] C. Yao, Q. Li, J. Guo, F. Yan, I. M. Hsing, *Adv. Healthcare Mater.* **2015**, *4*, 528.

[57] X. Gu, S. Y. Yeung, A. Chadda, E. N. Y. Poon, K. R. Boheler, I. M. Hsing, *Adv. Biosyst.* **2019**, *3*, 1800248.

[58] J. Rivnay, R. M. Owens, G. G. Malliaras, *Chem. Mater.* **2014**, *26*, 679.

[59] M. Sophocleous, L. Contat-Rodrigo, E. Garcia-Breijo, J. Georgiou, *IEEE Sens. J.* **2021**, *21*, 3977.

[60] S. Yeung, X. G. Y., C. M. Tsangb, S. W. Tsaoc, I. M. Hsing, *Sens. Actuators, A* **2019**, *287*, 185.

[61] L. H. Jimison, S. A. Tria, D. Khodagholy, M. Gurfinkel, E. Lanzarini, A. Hama, G. G. Malliaras, R. M. Owens, *Adv. Mater.* **2012**, *24*, 5919.

[62] F. Cicoira, M. Sessolo, O. Yaghmazadeh, J. A. DeFranco, S. Y. Yang, *Adv. Mater.* **2010**, *22*, 1012.

[63] M. Ramuz, K. Margita, A. Hama, P. Leleux, J. Rivnay, I. Bazin, R. M. Owens, *ChemPhysChem* **2015**, *16*, 1210.

[64] S. T. Tria, L. H. Jimison, A. Hama, M. Bongo, R. M. Owens, *Biochim. Biophys. Acta* **2013**, *1830*, 4381.

[65] a) C. Greulich, S. Kittler, M. Epple, G. Muhr, M. Köller, *Langenbecks Arch. Surg.* **2009**, *394*, 495; b) S. Kittler, C. Greulich, J. Diendorf, M. Koller, M. Epple, *Chem. Mater.* **2010**, *22*, 4548.

[66] F. Decataldo, M. Barbalinardo, D. Gentili, M. Tessarolo, M. Calienni, M. Cavallini, B. Fraboni, *Adv. Biosyst.* **2020**, *4*, 1900204.

[67] C. Yao, C. Xie, P. Lin, F. Yan, P. Huang, I. M. Hsing, *Adv. Mater.* **2013**, *25*, 6575.

[68] P. Lin, F. Yan, J. Yu, H. L. W. Chan, M. Yang, *Adv. Mater. Technol.* **2010**, *22*, 3655.

[69] V. F. Curto, B. Marchiori, A. Hama, A.-M. Pappa, M. P. Ferro, M. Braendlein, J. Rivnay, M. Fiocchi, G. G. Malliaras, M. Ramuz, R. M. Owens, *Microsyst. Nanoeng.* **2017**, *3*, 17028.

[70] a) F. Decataldo, V. Druet, A.-P. Pappa, E. Tan, A. Savva, C. Pitsalidis, S. Inal, J.-S. Kim, B. Fraboni, R. M. Owens, D. Iandolo, *Flexible Printed Electron.* **2019**, *4*, 044006; b) C. M. Proctor, J. Rivnay, G. G. Malliaras, *J. Polym. Sci., Part B: Polym. Phys.* **2016**, *54*, 1433; c) Y. Liang, M. Ernst, F. Brings, D. Kireev, V. Maybeck, A. Offenhäusser, D. Mayer, *Adv. Healthcare Mater.* **2018**, *7*, 1800304.

[71] M. Ramuz, A. Hama, J. Rivnay, P. Leleux, R. M. Owens, *J. Mater. Chem. B* **2015**, *3*, 5971.

[72] F. Decataldo, M. Barbalinardo, M. Tessarolo, V. Vurro, M. Calienni, D. Gentili, F. Valle, M. Cavallini, B. Fraboni, *Adv. Mater. Technol.* **2019**, *4*, 1900207.

[73] a) D. Koutsouras, A. Hama, J. Pas, P. Gkoupidenis, B. Hivert, C. Faivre-Sarrailh, E. Pasquale, R. M. Owens, G. G. Malliaras, *MRS Commun.* **2017**, *7*, 259; b) J. Pas, C. Pitsalidis, D. A. Koutsouras, P. P. Quilichini, F. Santoro, B. Cui, L. Gallais, R. P. O'Connor, G. G. Malliaras, R. M. Owens, *Adv. Biosyst.* **2018**, *2*, 1700164; c) P. Gkoupidenis, N. Schaefer, X. Strakosas, J. Fairfield, G. G. Malliaras, *Appl. Phys. Lett.* **2015**, *107*, 263302; d) P. Gkoupidenis, D. A. Koutsouras, G. G. Malliaras, *Nat. Commun.* **2017**, *8*, 15448.

[74] N. Y. Shim, D. A. Bernards, D. J. Macaya, J. A. DeFranco, M. Nikolou, R. M. Owens, G. G. Malliaras, *Sensors* **2009**, *9*, 9896.

[75] A. Campana, T. Cramer, D. T. Simon, M. Berggren, F. Biscarini, *Adv. Mater.* **2014**, *26*, 3874.

[76] W. Lee, D. Kim, J. Rivnay, N. Matsuhisa, T. Lonjaret, T. Yokota, H. Yawo, M. Sekino, G. G. Malliaras, T. Someya, *Adv. Mater.* **2016**, *28*, 9722.

[77] I. Gualandi, M. Marzocchi, E. Scavetta, M. Calienni, A. Bonfiglio, B. Fraboni, *J. Mater. Chem. B* **2015**, *3*, 6753.

[78] J. Liao, J. Lin, K. Liu, Y. Yang, R. Zhang, W. Du, X. Li, *Sens. Actuators, B* **2014**, *203*, 677.

[79] H. Tang, P. Lin, H. L. W. Chan, F. Yan, *Biosens. Bioelectron.* **2011**, *26*, 4559.

[80] E. Macchia, P. Romele, K. Manoli, M. Ghittorelli, M. Magliulo, Z. M. Kovács-Vajna, F. Torricelli, L. Torsi, *Flexible Printed Electron.* **2018**, *3*, 034002.

[81] L. V. Lingstedt, M. Ghittorelli, M. Brückner, J. Reinholz, N. I. Crăciun, F. Torricelli, V. Mailänder, P. Gkoupidenis, P. W. M. Blom, *Adv. Healthcare Mater.* **2019**, *8*, 1900128.

[82] J. M. Anderson, M. S. Balda, A. S. Fanning, *Curr. Opin. Cell Biol.* **1993**, *5*, 772.

[83] M. G. Farquhar, G. E. Palade, *J. Cell Biol.* **1963**, *17*, 375.

[84] J. M. Anderson, C. M. van Itallie, *Curr. Biol.* **1999**, *9*, R922.

[85] J. M. Anderson, *News Physiol. Sci.* **2001**, *16*, 126.

[86] a) L. González-Mariscal, P. Nava, S. Hernandez, *J. Membr. Biol.* **2005**, *207*, 55; b) T. Suzuki, *Cell. Mol. Life Sci.* **2013**, *70*, 631.

[87] J. M. Anderson, B. R. Stevenson, D. A. Goodenough, M. S. Mooseker, *J. Cell Biol.* **1986**, *103*, A71.

[88] A. S. Fanning, L. Mitic, J. M. Anderson, *J. Am. Soc. Nephrol.* **1999**, *10*, 1337.

[89] F. Ingels, S. Deferme, N. Delbar, M. Oth, P. Augustijns, *J. Pharm. Belg.* **2002**, *57*, 153.

[90] M. A. Deli, *Biochim. Biophys. Acta* **2009**, *1788*, 892.

[91] L. Gonzalez-Mariscal, *Tight junctions*, Landes Bioscience and Springer Science Business Media, USA **2006**.

[92] A. Fasano, *Physiol. Rev.* **2011**, *91*, 151.

[93] K. Sonaje, E.-Y. Chuang, K.-J. Lin, T.-C. Yen, F.-Y. Su, M. T. Tseng, H.-W. Sung, *Mol. Pharmaceutics* **2012**, *9*, 1271.

[94] B. Srinivasan, A. R. Kolli, M. B. Esch, H. E. Abaci, M. L. Shuler, J. J. Hickman, *J. Lab. Autom.* **2015**, *20*, 107.

[95] D. A. Koutsouras, L. V. Lingstedt, K. Lieberth, J. Reinholz, V. Mailänder, P. W. M. Blom, P. Gkoupidenis, *Adv. Healthcare Mater.* **2019**, *8*, 1901215.

[96] a) J. Wegener, D. Abrams, W. Willenbrink, H. J. Galla, A. Janshoff, *BioTechniques* **2004**, *37*, 590; b) J. Wegener, C. R. Keese, I. Giaever, *Exp. Cell Res.* **2000**, *259*, 158.

[97] a) K. Matter, M. S. Balda, *Int. Rev. Cytol.* **1999**, *1861*, 117; b) A. S. Fanning, C. M. van Itallie, J. M. Anderson, *Mol. Biol. Cell* **2012**, *23*, 577.

[98] A. M. Pappa, H. Y. Liu, W. Traberg-Christensen, Q. Thiburce, A. Savva, A. Pavia, A. Salleo, S. Daniel, R. M. Owens, *ACS Nano* **2020**, *14*, 12538.

[99] a) A. M. D. Wan, S. Inal, T. Williams, K. Wang, P. Leleux, L. Estevez, E. P. Giannelis, C. Fischbach, G. G. Malliaras, D. Gourdon, *J. Mater. Chem. B* **2015**, *3*, 5040; b) S. Inal, A. Hama, M. Ferro, C. Pitsalidis, J. Oziat, D. Iandolo, A.-M. Pappa, M. Hadida, M. Huerta, D. Marchat, P. Mailley, R. M. Owens, *Adv. Biosyst.* **2017**, *1*, 1700052.

[100] D. Gentili, P. D´Angelo, F. Militano, R. Mazzei, T. Poerio, M. Brucale, G. Tarabella, S. Bonetti, S. L. Marasso, M. Cocuzza, L. Giorno, S. Iannottab, M. Cavallini, *J. Mater. Chem. B* **2018**, *6*, 5400.

[101] a) M. H. Bolin, K. Svennersten, D. Nilsson, A. Sawatdee, E. W. Jager, A. Richter-Dahlfors, M. Berggren, *Adv. Mater.* **2009**, *21*, 4379; b) G. Tarabella, A. G. Balducci, N. Coppedè, S. L. Marasso, P. D'Angelo, S. Barbieri, M. Cocuzza, P. Colombo, F. Sonvico, R. Mosca, S. Iannotta, et al., *Biochim. Biophys. Acta* **2013**, *1830*, 4374.

[102] S. A. Tria, M. Ramuz, L. H. Jimison, A. Hama, R. M. Owens, *J. Vis. Exp.* **2014**, *84*, 2.

2100845 (14 of 16)

[103] S. Y. Yeunga, X. Gua, C. M. Tsang, S. W. G. Tsaoc, I. M. Hsing, *Sens. Actuators, B* **2019**, *297*, 126761.

[104] a) M. S. Balda, J. A., Whitney, C. Flores, S. Gonzilez, M. Cereijido, K. Matter, *J. Cell Biol.* **1996**, *134*, 1031; b) W. C. Prozialeck, J. R. Edwards, P. C. Lamar, C. S. Smith, *Toxicol. In Vitro* **2006**, *20*, 942.

[105] M. Braendlein, T. Lonjaret, P. Leleux, J.-M. Badier, G. G. Malliaras, *Adv. Sci.* **2017**, *4*, 1600247.

[106] M. Ghittorelli, L. Lingstedt, P. Romele, N. I. Cračiun, Z. M. Kovács-Vajna, P. W. M. Blom, F. Torricelli, *Nat. Commun.* **2018**, *9*, 1441.

[107] D. A. Bernards, G. G. Malliaras, *Adv. Funct. Mater.* **2007**, *17*, 3538.

[108] K. Lieberth, M. Brückner, F. Torricelli, V. Mailänder, P. Gkoupidenis, P. W. M. Blom, *Adv. Mater. Technol.* **2021**, *6*, 2000940.

[109] P. Romele, P. Gkoupidenis, D. A. Koutsouras, K. Lieberth, Z. M. Kovács-Vajna, P. W. Blom, F. Torricelli, *Nat. Commun.* **2020**, *11*, 3743.

[110] F. Torricelli, L. Colalongo, D. Raiteri, Z. M. Kovács-Vajna, E. Cantatore, *Nat. Commun.* **2016**, *7*, 10550.

[111] a) M. Sessolo, J. Rivnay, E. Bandiello, G. G. Malliaras, H. J. Bolink, *Adv. Mater. Interfaces* **2014**, *26*, 4803; b) K. Schmoltner, J. Kofler, A. Klug, E. J. W. List-Kratochvil, *Adv. Mater.* **2013**, *25*, 6895.

[112] P. Romele, M. Ghittorelli, Z. M. Kovács-Vajna, F. Torricelli, *Nat. Commun.* **2019**, *10*, 3044.

[113] a) E. Macchia, R. A. Picca, K. Kyriaki Manoli, C. Cinzia Di Franco, D. Davide Blasi, L. Lucia Sarcina, N. Nicoletta Ditaranto, N. Cioffi, R. Österbacka, G. Scamarcio, F. Torricell, L. Torsi, *Mater. Horiz.* **2020**, *7*, 999; b) R. A. Picca, K. Manoli, E. Macchia, L. Sarcina, C. Di Franco, N. Cioffi, D. Blasi, R. Österbacka, F. Torricelli, G. Scamarcio, L. Torsi, *Adv. Funct. Mater.* **2020**, *30*, 1904513.

[114] M. S. Balda, K. Matter, *Semin. Cell Dev. Biol.* **2000**, *11*, 281.

[115] a) G. McEwan, M. A. Jepson, B. H. Hirst, N. L. Simmons, *Biochim. Biophys. Acta* **1993**, *1148*, 51; b) R. F. Roblendo, M. W. D. S. Barber, *Toxicol. Sci.* **1999**, *51*, 119; c) G. Ranaldi, I. Marigliano, I. Vespignani, G. Perozzi, Y. Sambuy, *J. Nutr. Biochem.* **2002**, *13*, 157.

[116] a) I. Westergren, B. B. Johansson, *Acta Physiol. Scand.* **1993**, *149*, 99.; b) A. F. Kotzé, H. L. Luessen, B. J. de Leeuw, A. G. deBoer, J. C. Verhoef, H. E. Junginger, *J. Controlled Release* **1998**, *51*, 35; c) G. Sandri, P. Poggi, M. C. Bonferoni, S. Rossi, F. Ferrari, C. Caramella, *J. Pharm. Pharmacol.* **2006**, *58*, 1327.

[117] a) M. P. Deacon, S. MCGurk, C. J. Roberts, P. M. Williams, S. Tendler, M. C. Davies, S. S. Davis, S. E. Harding, *Biochem. J.* **2000**, *348*, 557; b) C.-M. Lehr, J. A. Bouwstra, E. H. Schacht, H. E. Junginger, *Int. J. Pharm.* **1992**, *78*, 43.

Katharina Lieberth received her bilingual B.Sc. degree in chemistry from AHU, Mulhouse, France and ALU, Freiburg, Germany in 2015. During Master's she was engaged in inorganic metallocene chemistry at Durham University, UK for her semester abroad, followed in 2018 by her graduation with a M.Sc. in chemistry from JMU, Würzburg, Germany. Her Master thesis focused on photoresist synthesis and its photolithographic performance at the Fraunhofer ISC in Würzburg. Currently, she is a Ph.D. candidate at the MPI for Polymer Research, Mainz, Germany, focusing on impedance sensing of cell tissues with organic electrochemical transistors for biomedical applications.

Fabrizio Torricelli received a D.Eng. degree with honors and a Ph.D. in electronics engineering from the University of Brescia (Italy) in 2006 and 2010, respectively. From 2010 to 2012, he was a post-doctoral fellow at the Eindhoven University of Technology, Netherlands. He was a consultant of ST-Microelectronics. Since 2019, he is associate professor at the Department of Information Engineering, University of Brescia. His research interests include device modeling, design of new memory and transistor architectures in silicon, metal-oxide and organic emerging technologies, and design and development of bioelectronics.

Paschalis Gkoupidenis earned his Ph.D. in materials science from NCSR "Demokritos," Athens, Greece, in 2014. During his Ph.D., his research focused on ionic transport mechanisms of organic electrolytes, for non-volatile memories. In 2015 he started a postdoc at the Department of Bioelectronics (EMSE, France), where he focused on the development of organic neuromorphic devices based on electrochemical concepts. In 2017, Gkoupidenis joined the Max Planck Institute for Polymer Research (Mainz, Germany), and he is currently a group leader at the Department of Molecular Electronics. The research in his group focuses on the area of organic neuromorphic electronics.

Paul W.M. Blom received his Ph.D. in 1992 from the Technical University Eindhoven on Picosecond Charge Carrier Dynamics in GaAs. At Philips Research Laboratories he was engaged in the electro-optical properties of polymer light-emitting diodes. From 2000 he held a professorship at the University of Groningen in the field of electrical and optical properties of organic semiconducting devices. In September 2008 he became Scientific Director of the Holst Centre in Eindhoven, where the focus was on foil-based electronics, followed in 2012 by an appointment as director at the MPI for polymer research in the field of molecular electronics.